

1 **Title: Many bat species are not potential hosts of SARS-CoV and SARS-CoV-**
2 **2: Evidence from ACE2 receptor usage**

3 **Authors:** Huan Yan^{1#}, Hengwu Jiao^{2#}, Qianyun Liu¹, Zhen Zhang¹, Xin Wang¹, Ming Guo¹,
4 Bing-Jun Wang², Ke Lan^{1,3*}, Yu Chen^{1*}, Huabin Zhao^{1,2*}

5 **Affiliations:**

6 ¹State Key Laboratory of Virology, Modern Virology Research Center, College of Life Sciences,
7 Wuhan University, Wuhan, 430072, China

8 ²Department of Ecology, Tibetan Centre for Ecology and Conservation at WHU-TU, Hubei Key
9 Laboratory of Cell Homeostasis, College of Life Sciences, Wuhan University, Wuhan 430072,
10 China

11 ³Frontier Science Center for Immunology and Metabolism, Wuhan University, Wuhan, 430072,
12 China

13
14 *Correspondence to: Huabin Zhao, Email: huabinzhao@whu.edu.cn; Yu Chen, Email:
15 chenyu@whu.edu.cn; Ke Lan, Email: kland@whu.edu.cn

16 #These authors contributed equally to this work.

17
18 **Abstract:** Bats are the suggested natural hosts for severe acute respiratory syndrome coronavirus
19 (SARS-CoV) and SARS-CoV-2, the latter of which caused the coronavirus disease 2019
20 (COVID-19) pandemic. The interaction of viral Spike proteins with their host receptor
21 angiotensin-converting enzyme 2 (ACE2) is a critical determinant of potential hosts and cross-
22 species transmission. Here we use virus-host receptor binding and infection assays to show that
23 ACE2 orthologs from 24, 21, and 16 of 46 phylogenetically diverse bat species – including those
24 in close and distant contact with humans – do not support entry of SARS-CoV, SARS-CoV-2,
25 and both of these coronaviruses, respectively. Furthermore, we used genetic and functional
26 analyses to identify genetic changes in bat ACE2 receptors associated with viral entry
27 restrictions. Our study demonstrates that many – if not most – bat species are not potential hosts
28 of SARS-CoV and SARS-CoV-2, and provides important insights into pandemic control and
29 wildlife conservation.

38 Introduction

39 The unprecedented pandemic of COVID-19, caused by the novel coronavirus SARS-CoV-2,
40 has led to major threats to public health and economic development. It is therefore critically
41 important to identify natural or intermediate hosts of SARS-CoV-2 to prevent further spread of
42 COVID-19 and future emergence of similar diseases. Inferred from sequence similarity of
43 human and bat virus genomes, it was suggested that horseshoe bats (*Rhinolophus* spp.) might be
44 natural hosts of SARS-CoV and SARS-CoV-2 (1-3). These suggestions have resulted in
45 misguided fears on all bats, and unwarranted attacks on many bats – including species other than
46 *Rhinolophus* – thereby seriously impacting efforts towards bat conservation (4). Given the
47 remarkable diversity of bats, which includes more than 1400 species across the globe (5),
48 assessing the possibility that diverse bat species act as potential hosts of SARS-CoV and SARS-
49 CoV-2 is urgent and crucial for both controlling outbreaks and protecting populations of wildlife.

50 ACE2 is the host cell receptor of SARS-CoV and SARS-CoV-2, and plays a vital role in
51 mediating viral entry to cause infection (1, 6). The interaction of a virus with its host receptor has
52 been repeatedly demonstrated to serve as a primary determinant of host range (7). Here we test
53 ACE2 orthologs from 46 bat species across the phylogeny, including species occurring in urban
54 and in rural areas, for their ability to support the entry of SARS-CoV and SARS-CoV-2. Hence,
55 this study assesses whether diverse bat species are potential hosts of SARS-CoV or SARS-CoV-
56 2. Moreover, by determining the correlation between proximity to humans and probability of
57 being natural hosts of the two viruses, these results provide important insights into pandemic
58 control and wildlife conservation.

59

60 Results

61 **Evolution of ACE2 in bats inhabiting urban or rural areas**

62 We collected ACE2 orthologs from 46 bat species across the phylogeny (**Figure 1 and**
63 **Table S1**). These species contained 28 species that roost or forage in urban areas in close
64 proximity to humans, and 18 species more restricted to rural areas and hence likely to have
65 minimal contact with humans (**Table S2**). In total, the examined species represent 11 bat families
66 that contain 1345 species, accounting for 96% of all bat species (**Table S3**). After aligning the
67 protein sequences of bat ACE2 orthologs, we examined 25 critical residues involved in the
68 binding of the surface spike glycoprotein (S protein) of SARS-CoV-2 (**Figure S1**) (8). Genetic
69 variations were observed in nearly all these 25 sites, which may have led to different abilities to
70 support entry of SARS-CoV and SARS-CoV-2 (8). Furthermore, we detected at least 22 amino
71 acid sites that are putatively under positive selection (**Table S4**), indicative of heterogeneous
72 selection pressure across sites. Notably, four of these positively selected sites are located in the
73 binding region of ACE2 to the SARS-CoV-2 S protein (**Table S4**).

74

75 **Interaction between bat ACE2 orthologs and SARS-CoV or SARS-CoV-2 receptor binding** 76 **domain (RBD)**

77 Efficient binding between the S protein and the ACE2 receptor is important for SARS-CoV
78 and SARS-CoV-2 entry. This binding is mainly mediated by the interaction between the critical
79 residues on the RBD and ACE2. To characterize the receptor function of ACE2 orthologs in a
80 range of diverse bat species, we generated a stable cell library consisting of cell lines expressing

81 the respective 46 bat ACE2 orthologs through lentiviral transduction of 293T cells lacking ACE2
82 expression (9). All bat ACE2 orthologs were exogenously expressed at a comparable level after
83 puromycin selection, as indicated by Western-blot and immunofluorescence assays detecting the
84 C-terminal 3×Flag tag (**Figure 2A-B**).

85 To analyze the interaction, we produced recombinant SARS or SARS-CoV-2 RBD human
86 IgG Fc fusion proteins (RBD-hFc), previously reported to be sufficient to bind human ACE2
87 efficiently (10, 11). The protein binding efficiency was tested on the bat ACE2 cell library
88 through immunofluorescence or flow cytometry targeting the human Fc. As expected, binding
89 was almost undetectable on mock 293T cells, but a strong binding signal was detected on the
90 293T cells expressing human ACE2 (**Figure 2C-D**). Consistent with previous reports (12, 13),
91 SARS-CoV-2 RBD showed higher binding to hACE2 than SARS-CoV, which can also be
92 observed on many bat ACE2 orthologs (**Figure 2C-D**). Previous reports have shown that only a
93 small fraction of ACE2 orthologs from tested mammalian species could not bind with SARS-
94 CoV-2 S protein [n=6 of 49 species (7); n=5 of 17 species (14)]. However, our study revealed
95 that many bat species (n=32 and n=28 of 46 species) do not support efficient binding with
96 SARS-CoV-RBD and SARS-CoV-2-RBD, respectively (**Figure 2C-D**). The overall profiles of
97 bat ACE2 to bind to SARS-CoV and SARS-CoV-2 RBD are generally comparable; a few
98 showed contrasting modes of binding preferences (**Figure 2C-D**). For instance, Bat22 can bind
99 to SARS-CoV but not SARS-CoV-2, whereas Bat14, 21, 40 can bind to SARS-CoV-2 but not
100 SARS-CoV (**Figure 2C-D**). Flow cytometry analysis showed consistent results (**Figure S2**).

101 Overall, the RBD-hFc binding assays demonstrated that bat ACE2 orthologs showed
102 different affinity and selectivity levels to SARS-CoV and SARS-CoV-2, indicating that ACE2
103 receptors of many bat species may not support efficient SARS-CoV and SARS-CoV-2 infection.

104

105 **Receptor function of bat ACE2 orthologs to support the entry of SARS-CoV and SARS-** 106 **CoV-2 using pseudotyped and live viruses**

107 To further evaluate the receptor function of different bat ACE2 orthologs, we employed a
108 Vesicular Stomatitis Virus (VSV)-based Rhabdoviral pseudotyping system for mimicking the
109 coronavirus spike-protein mediated single-round entry (14). SARS-CoV and SARS-CoV-2
110 pseudotypes were generated by assembling the coronavirus spike proteins and the replication-
111 deficient VSV with the VSV glycoprotein (VSVG) gene replaced with a fluorescence protein
112 (VSV-dG-GFP) or a Firefly Luciferase (VSV-dG-Luc) reporter (14). Both viruses showed
113 minimal background infection on 293T cells, but efficient infection on 293T-hACE2 cells
114 (**Figure S3**). The susceptibility of the 293T cells expressing bat ACE2 orthologs was then
115 examined with SARS-CoV and SARS-CoV-2 pseudotypes. The results showed that bat ACE2
116 orthologs have varying abilities to support coronavirus entry, and different preferences for
117 SARS-CoV and SARS-CoV-2. (**Figure 3A-B, Table S5**). Pseudotypes with GFP reporter
118 showed similar results (**Figure S4**). Notably, we found that 24, 21, and 16 of the 46 bat species
119 showed almost no entry for SARS-CoV, SARS-CoV-2, and both of these viruses, respectively
120 (**Figures 1 and 3A-B, Table S5**), suggesting that these species are not likely to be potential hosts
121 of either or both of these coronaviruses. The bat species showing no viral entry include those that
122 occur in urban areas as well as those more restricted to rural areas (**Figure 1, Table S1**),
123 suggesting that there is no correlation between proximity to humans and probability of being
124 natural hosts of SARS-CoV or SARS-CoV-2. Although horseshoe bats were suggested to be

125 potential natural hosts of SARS-CoV and SARS-CoV-2 (1-3), only one of the three examined
126 species (*Rhinolophus sinicus*) supported SARS-CoV entry; this species was suggested to be the
127 potential host of SARS-CoV (3, 15). None of these tested horseshoe bats showed entry for
128 SARS-CoV-2 (**Figures 1 and 3**). These results unambiguously indicate that ACE2 receptor
129 usage is species-dependent.

130 The SARS-CoV-2 S protein used here for pseudotyping contains a D614G mutation, which
131 is currently a dominant variation (16). The D614G mutation remarkably improved the *in vitro*
132 infectivity of SARS-CoV-2, but may not significantly affect the receptor interaction since it is
133 not in the RBD (17). Indeed, we identified a very similar susceptibility profile using an original
134 strain without D614G (**Figure S5**). We further demonstrated that the pseudotyped entry assay
135 mimics the entry of live viruses through a SARS-CoV-2 infection assay (**Figure 3C**). As
136 expected, the profile of SARS-CoV-2 N protein expression is highly consistent with the results
137 from the VSV-dG-based pseudotyped virus entry assay (**Figure 3C**). However, the live virus
138 infection resulted in the phenotype of plaque formation, while the pseudotypes showed evenly
139 distributed single-round infection (**Figure S4**).

140 When comparing the RBD-hFc binding and pseudotype entry profiles, we found that
141 binding and susceptibility are generally consistent, with a few exceptions. For instance, some
142 species (Bat12, 13, 14) were able to bind to SARS-CoV-2 RBD-hFc efficiently, but cannot
143 support infection of the same virus, indicating that high binding affinity does not guarantee
144 efficient viral entry (**Figures 2 and 3**). In contrast, some species (Bat3-8) were defective or less
145 efficient in SARS-CoV RBD-hFc binding, but supported the entry of the same virus to some
146 degree (**Figures 2 and 3**). We hypothesize that such minimal binding may be sufficient for viral
147 entry mediated by those ACE2 orthologs; alternatively, additional residues outside the traditional
148 RBD region might be required for efficient interaction. These hypotheses should be tested in the
149 future.

150 Together, our results demonstrated that SARS-CoV and SARS-CoV-2 can selectively use
151 some bat ACE2 as functional receptors for viral entry, but many – if not most – bat ACE2 are not
152 favored by one or both viruses. The functional defects in ACE2 coronavirus receptor in our
153 functional assays provide strong evidence that rejects the suggestion that many/most bat species
154 are potential natural hosts of SARS-CoV and/or SARS-CoV-2.

155

156 **Evaluation of critical genetic changes in bat ACE2 orthologs affecting the viral binding and** 157 **entry efficiency or specificity**

158 We comprehensively analyzed the relationship between critical RBD binding sites in bat
159 ACE2 sequences and their ability to support SARS-CoV and SARS-CoV-2 RBD binding and
160 viral entry. Several critical residues were identified that may play critical roles in the
161 determination of species specificity (**Figure S1**). According to the sequence alignment, two
162 species pairs (Bat33-34 and Bat38-40) were selected to demonstrate the role of critical residues
163 in RBD binding and viral entry, because they are phylogenetically close but show contrasting
164 phenotypes for supporting RBD binding and viral entry. Specifically, Bat34 and 38 do not
165 support SARS-CoV and SARS-CoV-2 RBD binding and infection, while Bat33 supports
166 efficient binding and infection of both viruses, and Bat40 supports infection of both viruses and
167 to a lesser degree, SARS-RBD binding (**Figures 2 and 3**). We compared their protein sequences
168 and highlighted the residues that may affect RBD interaction. For example, substitutions I27K,

169 N31G, and K42E were observed when comparing Bat33 and 34, while Q24L, E30K, K35Q, and
170 G354N were present between Bat38 and 40 (**Figure 4A**). We hypothesized that the discrepancy
171 in binding and infection phenotype is determined by their differences in critical residues for RBD
172 interaction. To test this hypothesis, we designed a residue swap mutagenesis assay to investigate
173 the role of critical residues on RBD binding and virus entry (**Figure 4A**). We generated four
174 swap mutations and corresponding 293T stable cell lines to test whether these substitutions can
175 achieve the gain-of-function and loss-of-function. All bat ACE2 orthologs and related mutants
176 were expressed at a comparable level after lentiviral transduction, as indicated by the
177 immunofluorescence of the carboxyl-terminal (C-terminal) 3×Flag tag (**Figure 4B**).
178 Recombinant SARS-CoV and SARS-CoV-2 RBD-hFc proteins were applied to the cells
179 expressing different ACE2, and the binding efficiency was evaluated by fluorescence (**Figure**
180 **4C**) and flow cytometry assays (**Figure 4D**). As expected, the swap of critical residues on the
181 selected four bat ACE2 changed their receptor function to the opposite, except for Bat38m
182 (Bat38 mutant) that remained unable to bind SARS-CoV RBD-hFc (**Figure 4D-4E**). The GFP
183 (**Figure 4E**) and Luciferase levels (**Figure 4F**) from the pseudotyped virus entry assay, as well
184 as the N protein staining from the live SARS-CoV-2 infection assay (**Figure 4G**) further
185 confirmed our hypothesis at the viral entry level. Structure modeling of bat ACE2 orthologs
186 showed that these residues appeared to occur in the interface between S protein and ACE2
187 receptor (**Figure 4H-4I**), and amino acid changes in these sites could potentially lead to different
188 abilities to support RBD binding and viral entry, confirming our results of virus-host receptor
189 binding and infection assays.

190

191 **Discussion**

192 Our study provides genetic and functional evidence from bat ACE2 receptor usage to reject
193 the suggestion that many, if not most, bat species are potential hosts of SARS-CoV and SARS-
194 CoV-2. Our sampling covers representative species from 11 bat families, accounting for 96% of
195 all extant bat species, hence providing a broad picture. Moreover, our study included 28 species
196 inhabiting urban areas and 18 species that are not common in cities or do not roost in buildings.
197 Our functional assays demonstrated that there is no correlation between proximity to humans and
198 probability of being natural hosts of SARS-CoV or SARS-CoV-2. Therefore, there is no need to
199 fear the many bat species occurring in cities that are not potential hosts of SARS-CoV and
200 SARS-CoV-2. Species such as horseshoe bats, which are suggested to be potential natural hosts
201 of the two viruses, should also not be feared, as they are less likely to be found in cities.

202 Our results are only partially consistent with a recently published prediction based on
203 sequence similarity, which estimated a binding score between ACE2 and the SARS-CoV-2 S
204 protein for each vertebrate species examined (8). The predicted binding scores for all 37 bat
205 species fell into low (n=8) and very low (n=29) categories (8), suggesting that all examined bat
206 species are at low risk for SARS-CoV-2 infection. Our study included 36 of the 37 previously
207 examined bat species (**Figure 1 and Table S1**); 19 of these appeared to support SARS-CoV-2
208 entry by their ACE2 receptors (**Figures 1 and 3**), strongly suggesting that these bats are at high
209 risk for SARS-CoV-2 infection. These disparities between in silico analyses and functional
210 experiments strongly indicate the importance of experimental data for confirmation of in silico
211 analyses, as our understanding of ACE2 sequences and structures is incomplete thus far. Indeed,
212 our genetic and functional evidence revealed critical residues of bat ACE2 that are involved in
213 supporting SARS-CoV-2 entry (**Figure 4**). However, these residues are not the genetic

214 determinant of New World monkey ACE2 orthologs mediating SARS-CoV-2 entry (7), and
215 many bat ACE2 orthologs carrying residues that were considered unfavorable in the same study
216 (H41 and E42) (7) were fully functional in our study (**Figure 4**), further confirming the
217 complexity of ACE2 functionality.

218 We found that closely related species can show strikingly different ACE2 receptor usage.
219 For example, *Rhinolophus sinicus* can support SARS-CoV entry, whereas its congeneric
220 relatives *R. ferrumequinum* and *R. pearsonii* cannot (**Figures 1 and 3**), despite the fact that some
221 polymorphic sites of ACE2 may have occurred in *R. sinicus* populations (18). These findings
222 clearly show that ACE2 receptor usage is species-dependent. Accordingly, although some bats
223 might be potential hosts of SARS-CoV and SARS-CoV-2 (1-3), one cannot assume that all bat
224 species or individuals can carry these viruses. On a positive note, even if some bat species are
225 potential hosts of certain viruses, they do not appear to have overt clinical signs of infection,
226 suggesting that these bats may serve as animal models to develop treatments for humans.
227 Although certain bat species are frequently observed to carry coronaviruses closely related to
228 human viruses in terms of sequence similarity (19), there is no solid and direct evidence showing
229 the initial spillover from bats to humans and other animals. Nevertheless, humans infected with
230 coronavirus should maintain distance from bats that can use ACE2 as a viral receptor, because
231 many bat species are endangered and may be susceptible to human coronaviruses (20), as
232 suggested for many other mammals (8, 21). Indeed, the International Union for Conservation of
233 Nature (IUCN) has assessed that over one third of bat species are threatened or data deficient,
234 and over half of all bat species have unknown or decreasing population trends (22). Thus, bats
235 are in need of protection more than ever.

236 Our study supports the calls that public education on bat biology will reduce the threat to
237 bats (4, 22). In fact, all bats are potentially safe as long as they are treated with care and respect.
238 We should work collaboratively to combat the pandemic and identify which species are potential
239 hosts, and not fear those species that are not hosts of the virus. Instead, we must respect and care
240 for those species that are potential hosts, and learn about the impact of human activities on their
241 natural habitats, which may lead to zoonotic spillover events.

242

243

244

245

246

247

248

249

250

251

252

253

254

References

- 255 1. P. Zhou, X. L. Yang, X. G. Wang, B. Hu, L. Zhang, W. Zhang, H. R. Si, Y. Zhu, B. Li, C.
256 L. Huang, H. D. Chen, J. Chen, Y. Luo, H. Guo, R. D. Jiang, M. Q. Liu, Y. Chen, X. R.
257 Shen, X. Wang, X. S. Zheng, K. Zhao, Q. J. Chen, F. Deng, L. L. Liu, B. Yan, F. X. Zhan,
258 Y. Y. Wang, G. F. Xiao, Z. L. Shi, A pneumonia outbreak associated with a new
259 coronavirus of probable bat origin. *Nature* **579**, 270-273 (2020).
- 260 2. W. Li, Z. Shi, M. Yu, W. Ren, C. Smith, J. H. Epstein, H. Wang, G. Cramer, Z. Hu, H.
261 Zhang, J. Zhang, J. McEachern, H. Field, P. Daszak, B. T. Eaton, S. Zhang, L. F. Wang,
262 Bats are natural reservoirs of SARS-like coronaviruses. *Science* **310**, 676-679 (2005).
- 263 3. B. Hu, L. P. Zeng, X. L. Yang, X. Y. Ge, W. Zhang, B. Li, J. Z. Xie, X. R. Shen, Y. Z.
264 Zhang, N. Wang, D. S. Luo, X. S. Zheng, M. N. Wang, P. Daszak, L. F. Wang, J. Cui, Z.
265 L. Shi, Discovery of a rich gene pool of bat SARS-related coronaviruses provides new
266 insights into the origin of SARS coronavirus. *PLoS Pathog* **13**, e1006698 (2017).
- 267 4. H. Zhao, COVID-19 drives new threat to bats in China. *Science* **367**, 1436 (2020).
- 268 5. D. E. Wilson, R. A. Mittermeier, *Handbook of the Mammals of the World. Vol. 9: Bats.*
269 (Lynx Edicions, Barcelona, 2019).
- 270 6. W. Li, M. J. Moore, N. Vasilieva, J. Sui, S. K. Wong, M. A. Berne, M. Somasundaran, J.
271 L. Sullivan, K. Luzuriaga, T. C. Greenough, H. Choe, M. Farzan, Angiotensin-converting
272 enzyme 2 is a functional receptor for the SARS coronavirus. *Nature* **426**, 450-454 (2003).
- 273 7. Y. Liu, G. Hu, Y. Wang, X. Zhao, F. Ji, W. Ren, M. Gong, X. Ju, C. Li, J. Hong, Y. Zhu,
274 X. Cai, J. Wu, X. Lan, Y. Xie, X. Wang, Z. Yuan, R. Zhang, Q. Ding, Functional and
275 genetic analysis of viral receptor ACE2 orthologs reveals broad potential host range of
276 SARS-CoV-2. *bioRxiv*, doi: <https://doi.org/10.1101/2020.1104.1122.046565> (2020).
- 277 8. J. Damas, G. M. Hughes, K. C. Keough, C. A. Painter, N. S. Persky, M. Corbo, M. Hiller,
278 K. P. Koepfli, A. R. Pfenning, H. Zhao, D. P. Genereux, R. Swofford, K. S. Pollard, O. A.
279 Ryder, M. T. Nweeia, K. Lindblad-Toh, E. C. Teeling, E. K. Karlsson, H. A. Lewin,
280 Broad host range of SARS-CoV-2 predicted by comparative and structural analysis of
281 ACE2 in vertebrates. *Proc Natl Acad Sci U S A*, <https://doi.org/10.1073/pnas.2010146117>
282 (2020).
- 283 9. E. C. Mossel, C. Huang, K. Narayanan, S. Makino, R. B. Tesh, C. J. Peters, Exogenous
284 ACE2 expression allows refractory cell lines to support severe acute respiratory
285 syndrome coronavirus replication. *J. Virol.* **79**, 3846-3850 (2005).
- 286 10. S. K. Wong, W. Li, M. J. Moore, H. Choe, M. Farzan, A 193-amino acid fragment of the
287 SARS coronavirus S protein efficiently binds angiotensin-converting enzyme 2. *J Biol*
288 *Chem* **279**, 3197-3201 (2004).
- 289 11. W. Tai, L. He, X. Zhang, J. Pu, D. Voronin, S. Jiang, Y. Zhou, L. Du, Characterization of
290 the receptor-binding domain (RBD) of 2019 novel coronavirus: implication for
291 development of RBD protein as a viral attachment inhibitor and vaccine. *Cell Mol*
292 *Immunol* **17**, 613-620 (2020).
- 293 12. D. Wrapp, N. Wang, K. S. Corbett, J. A. Goldsmith, C. L. Hsieh, O. Abiona, B. S.
294 Graham, J. S. McLellan, Cryo-EM structure of the 2019-nCoV spike in the prefusion
295 conformation. *Science* **367**, 1260-1263 (2020).
- 296 13. J. Shang, G. Ye, K. Shi, Y. Wan, C. Luo, H. Aihara, Q. Geng, A. Auerbach, F. Li,
297 Structural basis of receptor recognition by SARS-CoV-2. *Nature* **581**, 221-224 (2020).
- 298 14. J. Nie, Q. Li, J. Wu, C. Zhao, H. Hao, H. Liu, L. Zhang, L. Nie, H. Qin, M. Wang, Q. Lu,
299 X. Li, Q. Sun, J. Liu, C. Fan, W. Huang, M. Xu, Y. Wang, Establishment and validation

- 300 of a pseudovirus neutralization assay for SARS-CoV-2. *Emerg Microbes Infect* **9**, 680-
301 686 (2020).
- 302 15. S. K. Lau, P. C. Woo, K. S. Li, Y. Huang, H. W. Tsoi, B. H. Wong, S. S. Wong, S. Y.
303 Leung, K. H. Chan, K. Y. Yuen, Severe acute respiratory syndrome coronavirus-like
304 virus in Chinese horseshoe bats. *Proc Natl Acad Sci U S A* **102**, 14040-14045 (2005).
- 305 16. B. Korber, W. M. Fischer, S. Gnanakaran, H. Yoon, J. Theiler, W. Abfalterer, N.
306 Hengartner, E. E. Giorgi, T. Bhattacharya, B. Foley, K. M. Hastie, M. D. Parker, D. G.
307 Partridge, C. M. Evans, T. M. Freeman, T. I. de Silva, C.-G. G. Sheffield, C. McDanal, L.
308 G. Perez, H. Tang, A. Moon-Walker, S. P. Whelan, C. C. LaBranche, E. O. Saphire, D. C.
309 Montefiori, Tracking changes in SARS-CoV-2 spike: Evidence that D614G increases
310 infectivity of the COVID-19 virus. *Cell* **182**, 812-827 e819 (2020).
- 311 17. J. Hu, C. L. He, Q. Z. Gao, G. J. Zhang, X. X. Cao, Q. X. Long, H. J. Deng, L. Y. Huang,
312 J. Chen, K. Wang, N. Tang, A. L. Huang, The D614G mutation of SARS-CoV-2 spike
313 protein enhances viral infectivity and decreases neutralization sensitivity to individual
314 convalescent sera. *bioRxiv*, doi: <https://doi.org/10.1101/2020.1106.1120.161323> (2020).
- 315 18. H. Guo, B. J. Hu, X. L. Yang, L. P. Zeng, B. Li, S. Ouyang, Z. L. Shi, Evolutionary arms
316 race between virus and host drives genetic diversity in bat SARS related coronavirus
317 spike genes. *J. Virol.*, <https://doi.org/10.1128/JVI.00902-00920> (2020).
- 318 19. A. Banerjee, K. Kulcsar, V. Misra, M. Frieman, K. Mossman, Bats and Coronaviruses.
319 *Viruses* **11**, 41 (2019).
- 320 20. K. J. Olival, P. M. Cryan, B. R. Amman, R. S. Baric, D. S. Blehert, C. E. Brook, C. H.
321 Calisher, K. T. Castle, J. T. H. Coleman, P. Daszak, J. H. Epstein, H. Field, W. F. Frick,
322 A. T. Gilbert, D. T. S. Hayman, H. S. Ip, W. B. Karesh, C. K. Johnson, R. C. Kading, T.
323 Kingston, J. M. Lorch, I. H. Mendenhall, A. J. Peel, K. L. Phelps, R. K. Plowright, D. M.
324 Reeder, J. D. Reichard, J. M. Sleeman, D. G. Streicker, J. S. Towner, L. F. Wang,
325 Possibility for reverse zoonotic transmission of SARS-CoV-2 to free-ranging wildlife: A
326 case study of bats. *PLoS Pathog* **16**, e1008758 (2020).
- 327 21. J. Z. Shi, Z. Y. Wen, G. X. Zhong, H. L. Yang, C. Wang, B. Y. Huang, R. Q. Liu, X. J.
328 He, L. Shuai, Z. R. Sun, Y. B. Zhao, P. P. Liu, L. B. Liang, P. F. Cui, J. L. Wang, X. F.
329 Zhang, Y. T. Guan, W. J. Tan, G. Z. Wu, H. L. Chen, Z. G. Bu, Susceptibility of ferrets,
330 cats, dogs, and other domesticated animals to SARS-coronavirus 2. *Science* **368**, 1016-
331 1020 (2020).
- 332 22. W. F. Frick, T. Kingston, J. Flanders, A review of the major threats and challenges to
333 global bat conservation. *Ann N Y Acad Sci*, <https://doi.org/10.1111/nyas.14045> (2019).
- 334 23. R. C. Edgar, MUSCLE: multiple sequence alignment with high accuracy and high
335 throughput. *Nucleic Acids Res.* **32**, 1792-1797 (2004).
- 336 24. B. Xu, Z. Yang, PAMLX: a graphical user interface for PAML. *Mol. Biol. Evol.* **30**,
337 2723-2724 (2013).
- 338 25. E. C. Teeling, M. S. Springer, O. Madsen, P. Bates, S. J. O'Brien, W. J. Murphy, A
339 molecular phylogeny for bats illuminates biogeography and the fossil record. *Science* **307**,
340 580-584 (2005).
- 341 26. F. C. Almeida, N. B. Simmons, N. P. Giannini, A species-level phylogeny of Old World
342 fruit bats with a new higher-level classification of the family Pteropodidae. *Am Mus Novit*,
343 3950 (2020).
- 344 27. D. Rojas, O. M. Warsi, L. M. Davalos, Bats (Chiroptera: Noctilionoidea) challenge a
345 recent origin of extant neotropical diversity. *Syst. Biol.* **65**, 432-448 (2016).

- 346 28. S. Fukushi, T. Mizutani, M. Saijo, S. Matsuyama, N. Miyajima, F. Taguchi, S. Itamura, I.
347 Kurane, S. Morikawa, Vesicular stomatitis virus pseudotyped with severe acute
348 respiratory syndrome coronavirus spike protein. *J Gen Virol* **86**, 2269-2274 (2005).
- 349 29. C. Schwegmann-Wessels, J. Glende, X. Ren, X. Qu, H. Deng, L. Enjuanes, G. Herrler,
350 Comparison of vesicular stomatitis virus pseudotyped with the S proteins from a porcine
351 and a human coronavirus. *J Gen Virol* **90**, 1724-1729 (2009).
- 352 30. M. A. Whitt, Generation of VSV pseudotypes using recombinant DeltaG-VSV for studies
353 on virus entry, identification of entry inhibitors, and immune responses to vaccines. *J.*
354 *Virol. Methods* **169**, 365-374 (2010).
- 355 31. J. Yang, R. Yan, A. Roy, D. Xu, J. Poisson, Y. Zhang, The I-TASSER Suite: protein
356 structure and function prediction. *Nat Methods* **12**, 7-8 (2015).
- 357 32. Y. Zhang, I-TASSER server for protein 3D structure prediction. *BMC Bioinformatics* **9**,
358 40 (2008).
- 359 33. S. Yuan, H. C. S. Chan, S. Filipek, H. Vogel, PyMOL and Inkscape bridge the data and
360 the data visualization. *Structure* **24**, 2041-2042 (2016).

361

362

363 **Acknowledgments:** We thank B. Fenton, L. Moretoo, and D.M. Morales-Mart ínez for sharing
364 their knowledge as to whether certain bats roost or forage in cities, Prof. Zheng-Li Shi for
365 providing the SARS-CoV-2 virus, and Ming Dai, Zhixiang Huang, Yan Rao, Jing Zhang, and
366 Bei Wang from ABSL-3 Laboratory of Wuhan University for their technical support. We are
367 grateful to Beijing Taikang Yicai Foundation for their great support to this work. **Funding:** This
368 study was supported by Special Fund for COVID-19 Research of Wuhan University, China
369 NSFC grants (31722051 and 32041007), China National Science and Technology Major Project
370 (2018ZX10733403). **Author contributions:** H.Z., H.Y., Y.C., and K.L. designed study; H.Z.,
371 H.Y., H.J. wrote manuscript; H.Y., H.J., Q.L., Z.Z., X.W., and M.G. performed experiments;
372 H.Y., H.Z., H.J., and Y.C. analyzed data. **Competing interests:** None of the authors have any
373 competing interests. **Data and materials availability:** All data are available in the manuscript or
374 the supplementary materials.

375

376 **Materials and Methods**

377 **ACE2 sequence acquisition and selective pressure analysis**

378 We obtained 46 full-length coding sequences of bat *ACE2* in this study, of which 32 were
379 taken from a recent study (8), and 14 were newly extracted from published or recently sequenced
380 genome assemblies (see **Table S1** for the sources and accession numbers for the sequences and
381 assemblies). Next, we aligned the deduced *ACE2* protein sequences using the MUSCLE program
382 (23) (see **Figure S1** for the resulting alignment). The sequence logo was generated with
383 WebLogo (<https://weblogo.berkeley.edu/logo.cgi>). We performed selective pressure analysis on
384 bat *ACE2* using CodeML implemented in PAML (24). Two comparisons of site models (M1a &
385 M2a, M8a & M8) were used to predict positively selected sites (24). The input tree was the
386 species tree (**Figure 1**) taken from previous studies (25-27).

387

388 **Cell culture**

389 HEK293T cells (293T, ATCC, CRL-3216) and VERO-E6 cells (ATCC, CRL-1586) were
390 cultured in Dulbecco's modified Eagle's medium (DMEM; Gibco) supplemented with 10% fetal
391 bovine serum (FBS), 2.0 mM L-Glutamine, 110 mg/L sodium pyruvate, and 4.5 g/L D-glucose.
392 11-Hybridoma (CRL-2700) secreting a monoclonal antibody targeting against VSV glycoprotein
393 was cultured in Minimum Essential Medium with Earle's salts and 2.0 mM L-Glutamine (MEM;
394 Gibco). All cells were cultured at 37°C in 5% CO₂ with the regular passage of every 2-3 days.
395 293T stable cell lines overexpressing ACE2 orthologs were maintained in growth medium
396 supplemented with 1 µg/ml puromycin.

397

398 **Plasmids**

399 Human codon-optimized cDNA sequences encoding various ACE2 orthologs and their
400 mutants fused with a C-terminus 3×Flag tag (DYKDHD-G-DYKDHD-I-DYKDDDDK) were
401 commercially synthesized and subcloned into a lentiviral transfer vector (pLVX-IRES-puro)
402 through the EcoRI and NotI restriction sites. The DNA sequences of human codon-optimized
403 SARS-CoV S protein (CUHK-W1, GenBank: AY278554.2) and SARS-CoV-2 S protein
404 (Wuhan-Hu-1, GenBank: MN908947) were amplified from plasmids pCMV/hygro-SARS-CoV-
405 S (VG40150-G-N, Sino Biological, China) and pCAGGS-SARS-CoV-2-S-c9 (gifted from Dr.
406 Wenhui Li, National Institute of Biological Science, Beijing, China) into pCAGGS vector with
407 C-terminal 18 aa deletion for improving VSV pseudotyping efficiency (28, 29). The D614G
408 mutation was introduced into the SARS-CoV-2-S coding sequence to improve *in vitro* infection
409 efficiency. The plasmids for the expression of coronavirus RBD-IgG Fc fusion proteins were
410 generated by inserting the coding sequences of SARS-CoV RBD (aa 318-516) and SARS-CoV-2
411 RBD (aa331-530) into the pCAGGS vector to express fusion proteins with C-terminal human Fc
412 (IgG1) and N-terminal CD5 secretion leading sequence (MPMGSLQPLATLYLLGMLVASVL).

413

414 **Generation of ACE2 stable expression cell lines**

415 293T cells overexpressing ACE2 orthologs were generated by lentiviral transduction.
416 Specifically, the lentivirus was produced by cotransfection of lentiviral transfer vector carrying
417 ACE2 coding sequences (pLVX-EF1a-Puro, from Genewiz Inc.) and packaging plasmids
418 pMD2G (Addgene #12259) and psPAX2 (Addgene #12260) into 293T cells through
419 Lipofectamine 3000 (Thermo Fisher Scientific, United States). The lentivirus-containing
420 supernatant was collected and pooled at 24 and 48 hours (hrs) post-transfection. HEK293T cells
421 were transduced by the lentivirus after 16 hrs, in the presence of 8 µg/ml polybrene. Stable cells
422 expressing various ACE2 orthologs were selected and maintained in growth medium with
423 puromycin (1 µg/ml).

424

425 **Immunofluorescence assay to evaluate the expression level of ACE2 orthologs**

426 The expression levels of ACE2 orthologs were evaluated by the immunofluorescence assay
427 detecting the C-terminal 3×Flag tags. The cells for analysis were seeded in the poly-lysine
428 pretreated 96-well plate at a cell density of 5×10⁵/ml (100 µl/well), and cultured for 24 hrs. Cells
429 were fixed with 4% paraformaldehyde at room temperature for 10 mins, permeablized with 0.2%

430 Triton X-100/PBS at room temperature for 10 mins, and blocked with 1% Bovine serum albumin
431 (BSA) at 37°C for 30 mins. Next they were incubated with the mouse monoclonal antibody
432 targeting Flag tag (9A3, #8146S, Cell signaling technology, United States) diluted in 1%
433 BSA/PBS at 37°C for 1 hour. After three rounds of PBS washing, cells were subsequently
434 incubated with 2 µg/ml of the secondary goat anti-rabbit antibody conjugated with Alexa Fluor
435 594 (A11032, Thermo Fisher Scientific, United States) diluted in 1% BSA /PBS at room
436 temperature for 30 mins. The nucleus was stained with Hoechst 33342 (1:5000 dilution in PBS)
437 in blue. Images were captured with a fluorescence microscope (MI52-N, Mshot, China).

438

439 **Production of VSV reporter virus pseudotyped with coronavirus spike proteins**

440 Coronavirus spike protein pseudotyped virus (CoV-psV) were packaged following a
441 previously described protocol using a replicate-deficient VSV based rhabdoviral pseudotyping
442 system (VSV-dG) (30). The VSV-G glycoprotein deficient VSV exogenously expressing EGFP
443 (VSV-dG-GFP) or Firefly Luciferase (VSV-dG-Luc) were rescued by a reverse genetics system
444 purchased from a company (Kerafast). To produce CoV-psV, Vero-E6 cells were transfected
445 with the plasmids overexpressing SARS2-CoV (pCAGGS-SARS-S-dc) and SARS2-CoV-2 spike
446 proteins (pCAGGS-SARS2-S-dc) through Lipofectamine 3000 reagent. After 36 hrs, the
447 transfected cells were transduced with VSV-dG reporter viruses diluted in serum-free opti-MEM
448 for 1 hour at 37°C (MOI=10). The transduced cells were washed with culture medium once and
449 then replenished with fresh culture medium with L1 hybridoma cultured supernatant containing
450 anti-VSV mAb (1:100 dilution) to neutralize the infectivity of the residual input viruses. The
451 CoV-psV containing supernatants were harvested at 24 hrs after transduction, clarified at 12,000
452 rpm for 2 mins at 4°C, and immediately transferred to -80°C for storage. The viral titer (genome
453 equivalents) was determined by quantitative reverse transcription PCR (RT-qPCR). The RNA
454 copies in the virus-containing supernatant were detected using the VSV-L gene sequences.

455

456 **Pseudotype entry assay**

457 293T stable cell lines overexpressing various ACE2 orthologs were trypsinized and
458 resuspended together with SARS-CoV or SARS-CoV-2 pseudotyped viruses (at a genome
459 equivalents=100) in DMEM with 10% FBS. Next they were seeded at 5×10^4 in a well of a 96-
460 well plate to allow attachment and viral infection simultaneously. At 16-24 hrs after infection,
461 images of infected cells with GFP expression were acquired with a fluorescence microscope
462 (MI52-N, Mshot, China). Cells infected with pseudovirus expressing firefly luciferase were
463 lysed by $1 \times$ passive lysis buffer (Promega, United States) at room temperature for 15 mins.
464 Luciferase activity in the cell lysate was determined by a Bright-Glo luciferase assay kit
465 (Promega, United States) and measured through a Spectra MaxiD3 multi-well Luminometer
466 (Molecular Devices, United States) or a GloMax® 20/20 Luminometer (Promega, United States).

467

468 **Coronavirus RBD-hFc binding assay**

469 Recombinant SARS-CoV-RBD-hFc and SARS-CoV-2-RBD-hFc proteins were produced
470 by transient transfection of 293T cells with Lipofectamine 3000. The transfected cells were
471 cultured in Free-style 293 serum-free medium (Thermo Scientific), and the supernatants
472 containing the recombinant proteins were collected at 2 and 4 days post-transfection. The RBD-

473 hFc protein concentration was determined by comparing the target protein band with BSA
474 standard dilutions through Coomassie staining. The RBD-hFc protein-containing supernatant
475 was diluted with culture medium (5-10 µg/ml) and then incubated with the 293T stable cell line
476 overexpressing different ACE2 orthologs for 1 hour at 37°C. Cells were washed twice with
477 DMEM and then incubated with 2 µg/ml of Alexa Fluor 488 conjugated Goat anti-Human IgG
478 (A11013, Thermo Fisher Scientific, United States) diluted in DMEM with 2% FBS for 30 mins
479 at 37°C. For immunostaining, cells were washed twice with PBS and incubated with PBS with
480 Hoechst 33342 (1:5000 dilution in PBS) for nucleus staining. Images were captured with a
481 fluorescence microscope (MI52-N, Mshot, China). For flow cytometry analysis, cells were
482 detached by 5mM EDTA/PBS and analyzed with a CytoFLEX Flow Cytometer
483 (Beckman Coulter, United States).

484

485 **SARS-CoV-2 live virus infection assay**

486 The SARS-CoV-2 (strain IVCAS 6.7512) was provided by the National Virus Resource,
487 Wuhan Institute of Virology, Chinese Academy of Sciences. All SARS-CoV-2 live virus related
488 experiments were approved by the Biosafety Committee Level 3 (ABSL-3) of Wuhan University.
489 All experiments involving SARS-CoV-2 were performed in the BSL-3 facility. SARS-CoV-2
490 was amplified on Vero-E6 cells and stored at -150°C, and the titer was determined on Vero-E6
491 cells through a plaque assay. 293T cells expressing ACE2 orthologs were seeded on a poly-
492 lysine coated 96-well plate for 24 hrs before inoculation. Cells were infected with SARS-CoV-2
493 at MOI=0.01, and then incubated in DMEM with 2% FBS for 48 hrs before testing. The cells
494 were fixed with 4% paraformaldehyde in PBS at room temperature for 1 hour, permeabilized with
495 0.2% Triton X-100 for 10 mins, and then blocked with 1% BSA/PBS at 37°C for 1 hour. Cells
496 were subsequently incubated with a mouse monoclonal antibody SARS-CoV/SARS-CoV-2
497 Nucleocapsid Antibody (40143-MM05, Sino Biological, China) at 1:500 at 37°C for 1 hour, and
498 then incubated with 2µg/ml of goat anti-mouse secondary antibody, Alexa Fluor 594 (A-11032,
499 Thermo Fisher Scientific) at 37°C for 1 hour. The nucleus was stained with Hoechst 33342.
500 Images were acquired with a fluorescence microscope (MI52-N, Mshot, China).

501

502

503 **Homology-based structural modeling**

504 Molecular models of different bat ACE2 were predicted by I-TASSER (Iterative
505 Threading ASSEmbly Refinement) version 5.1 (31). Starting from the amino acid sequences, the
506 I-TASSER algorithm constructed the full-length 3D atomic models by structural template
507 identification, followed by template-based fragment assembly simulations. The model with the
508 highest confidence score in each prediction was used for subsequent analyses (32). Only the
509 predicted structures of the N-terminal peptidase domain (PD) of ACE2 were used in the analyses.
510 The structural alignment and visualization were implemented in PyMOL (33).

511

512 **Statistical analysis:**

513 Data are expressed as mean values with standard deviation. All experiments were
514 repeated 3-5 times, each yielding similar results.

515 **Figure legends:**

516 **Fig. 1. Phylogenetic tree of 46 bat species in this study.** Labels of bat species in our
517 experiments are indicated. Infection abilities of bat ACE2 to support SARS-CoV and SARS-
518 CoV-2 entry are shown with different signs: infection data are indicated as % mean values of bat
519 ACE2 supporting infection compared with the infection supported by human ACE2; infection
520 efficiency smaller than 5% is indicated with a minus sign (-), between 5% and 50% a plus sign
521 (+), and greater than 50% a double plus sign (++). Labels shown in bold indicate the bat species
522 that have been examined by in silico analyses in a recent study (8). Bat phylogeny was taken
523 from previous studies (25-27).

524
525 **Fig. 2. Expression of bat ACE2 orthologs and their interaction with SARS-CoV and SARS-
526 CoV-2 RBD.** (A) Western blot detecting the expression levels of ACE2 orthologs on 293T stable
527 cells by targeting the C-terminal Flag tag. Glyceraldehyde 3-phosphate dehydrogenase (GAPDH)
528 was employed as a loading control. (B) Visualization of the intracellular bat ACE2 expression
529 level by immunofluorescence assay detecting the C-terminal Flag tag. Scale bar=100 μ m. (C-D)
530 Assessment of the interaction between different ACE2 orthologs and SARS-CoV-RBD-hFc (C)
531 or SARS-CoV-2-RBD-hFc (D). Species that do not support efficient binding are underlined.
532 293T cells stably expressing the different bat ACE2 orthologs were incubated with 5 μ g/ml of
533 the recombinant proteins at 37°C for 1 h. The binding efficiency was examined by Alexa Fluor-
534 488 Goat anti-human IgG through fluorescence assay. Scale bar=200 μ m.

535
536 **Fig. 3. Characterization of bat ACE2 orthologs mediating entry of SARS-CoV and SARS-
537 CoV-2 viruses.** (A-B) The ability of bat ACE2 orthologs to support the entry of SARS-CoV and
538 SARS-CoV-2 pseudovirus. 293T cells expressing bat ACE2 orthologs in a 96-well plate were
539 infected with SARS-CoV (A) and SARS-CoV-2 (B) spike protein pseudotyped VSV-dG-Luc.
540 The luciferase activity of the cell lysate was determined at 20 hours post-infection (hpi). (C)
541 293T cells expressing bat ACE2 orthologs were inoculated with the SARS-CoV-2 live virus at
542 MOI=0.01. N proteins (red) in the infected cells were detected by an immunofluorescence assay
543 at 48 hpi. Scale bar=200 μ m. Species that show almost no entry for SARS-CoV-2 live virus are
544 underlined.

545
546 **Fig. 4. Evaluation of the critical binding sites determining the species-specific restriction of
547 SARS-CoV and SARS-CoV-2 binding and entry.** (A) Swap mutagenesis assay to investigate
548 the role of critical binding sites on bat ACE2 orthologs for tropism determination. Residues
549 involved in RBD (according to the structure between SARS2-RBD and human ACE2, PDB:
550 6M0J) interaction are shown in the table. Residues that changed in the mutagenesis assay are
551 marked in red. (B) The expression level of the bat ACE2 orthologs and related mutants in
552 transduced 293T cells was determined by an immunofluorescence assay recognizing the Flag tag.
553 Scale bar=200 μ m. (C-D) Binding efficiency of SARS2-RBD-hFc and SARS2-RBD-hFc on
554 293T cells expressing bat ACE2 and related mutants. Cells were incubated with 5 μ g/ml of
555 recombinant proteins at 37 °C for 1 hour, and then washed and incubated with a secondary
556 antibody recognizing human Fc. Immunostaining (C) and flow cytometry (D) were conducted to
557 show the binding efficiency. Scale bar=200 μ m. (E-F) The ability of the indicated ACE2 and
558 related mutants to support the entry of coronavirus pseudotypes. The 293T cells expressing the

559 indicated ACE2 and their mutants were infected by SARS-CoV and SARS-CoV-2 pseudotypes
560 expressing GFP (E) and luciferase (F). Infection was analyzed at 20 hpi. Scale bar=200 μm . (G)
561 293T cells infected by the SARS-CoV-2 live virus at MOI=0.01; the infection was examined at
562 48 hpi through N protein (red) immunostaining. Nuclei were stained with Hoechst 33342 in blue.
563 Scale bar=200 μm . (H) Structure alignment for the Bat33 ACE2-PD (cyan) and Bat34 ACE2-PD
564 (wheat). The regions enclosed by the blue-dashed lines are illustrated in detail in the right, in
565 which the variation of the interface residues between Bat33 ACE2-PD (cyan) and Bat34 ACE2-
566 PD (wheat) are indicated by different side chains. (I) Structural alignment for the Bat38 ACE2-
567 PD (cyan) and Bat40 ACE2-PD (wheat). The regions enclosed by the purple dashed lines are
568 illustrated in detail in the right, in which the variation of the interface residues between Bat38
569 ACE2-PD (cyan) and Bat40 ACE2-PD (wheat) are indicated by different side chains.

570

571

Figure 1

bioRxiv preprint doi: <https://doi.org/10.1101/2020.09.08.284737>; this version posted September 10, 2020. The copyright holder for this preprint (which was not certified by peer review) is the author/funder, who has granted bioRxiv a license to display the preprint in perpetuity. It is made available under a [CC-BY-NC-ND 4.0 International license](#).

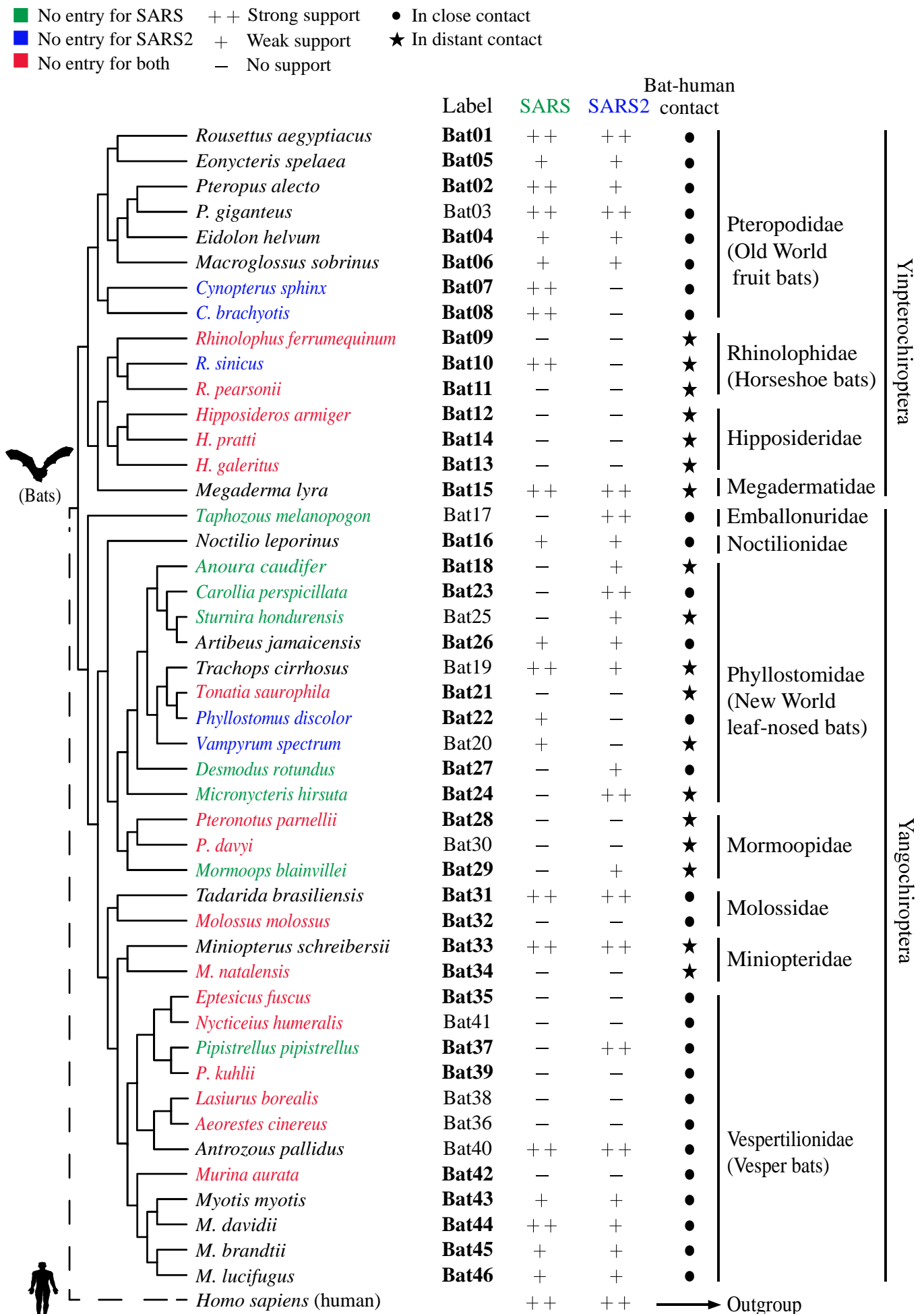


Figure 2

bioRxiv preprint doi: <https://doi.org/10.1101/2020.09.08.284737>; this version posted September 10, 2020. The copyright holder for this preprint (which was not certified by peer review) is the author/funder, who has granted bioRxiv a license to display the preprint in perpetuity. It is made available under a [CC-BY-NC-ND 4.0 International license](https://creativecommons.org/licenses/by-nc-nd/4.0/).

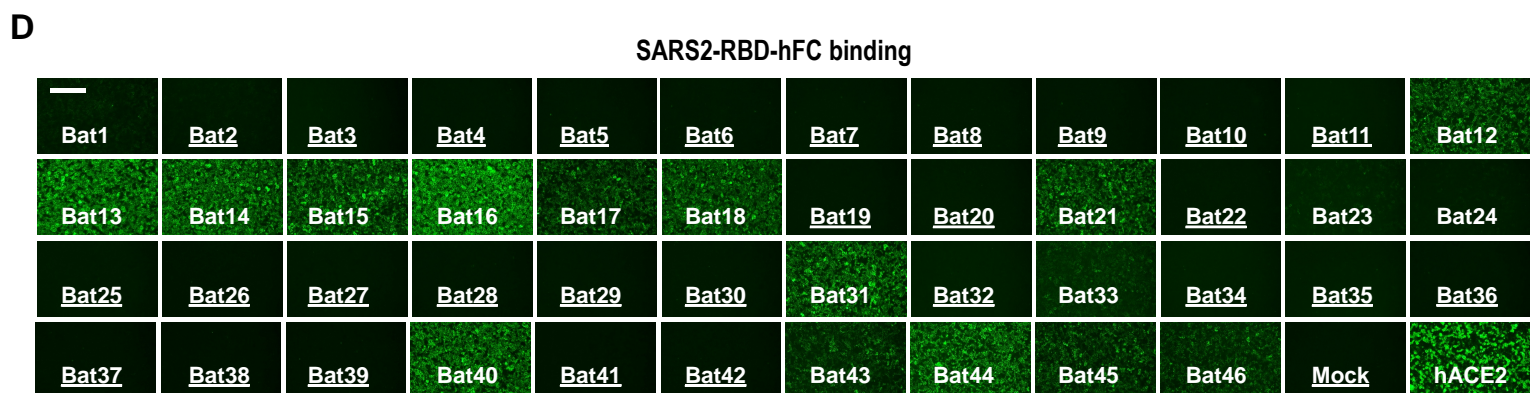
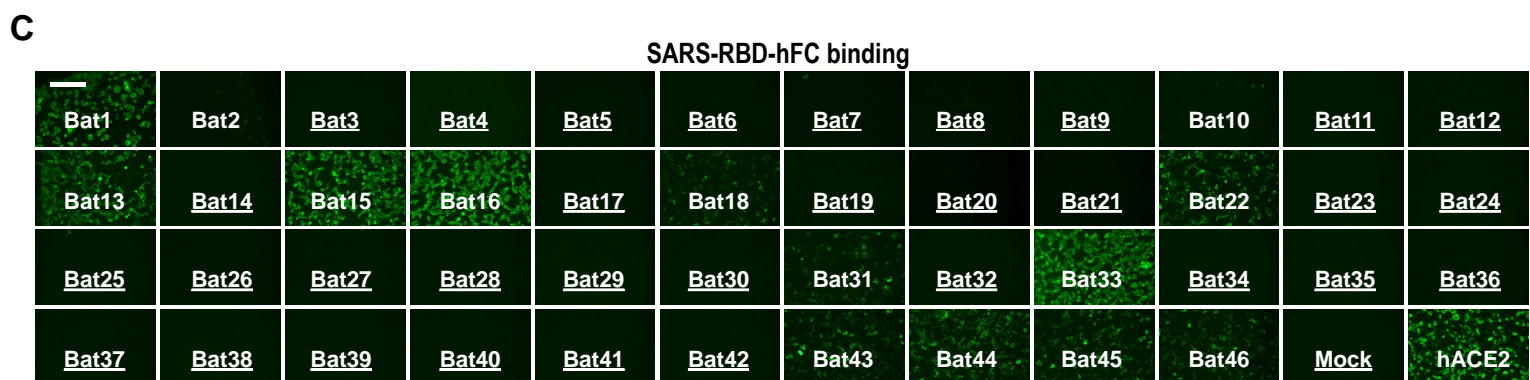
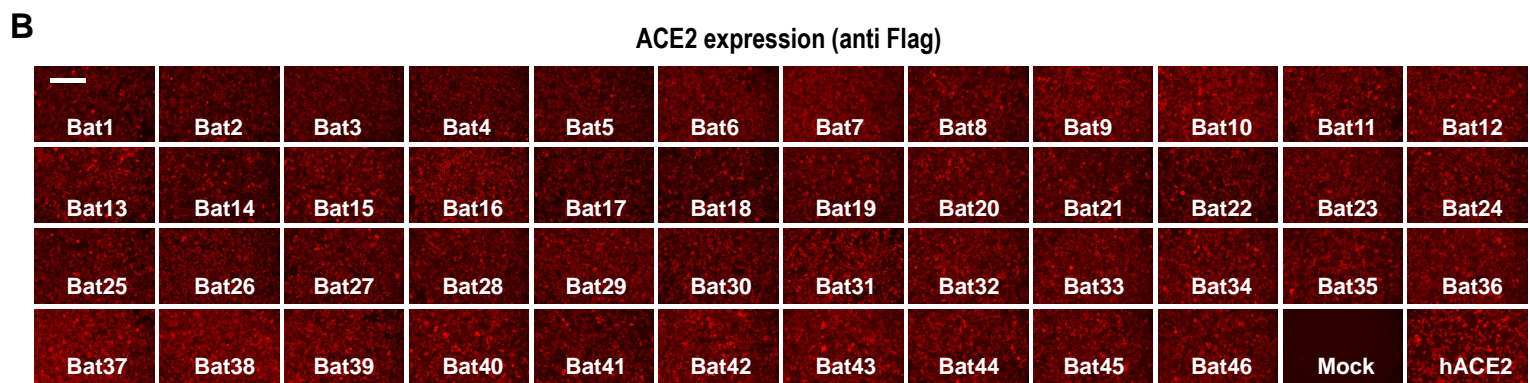
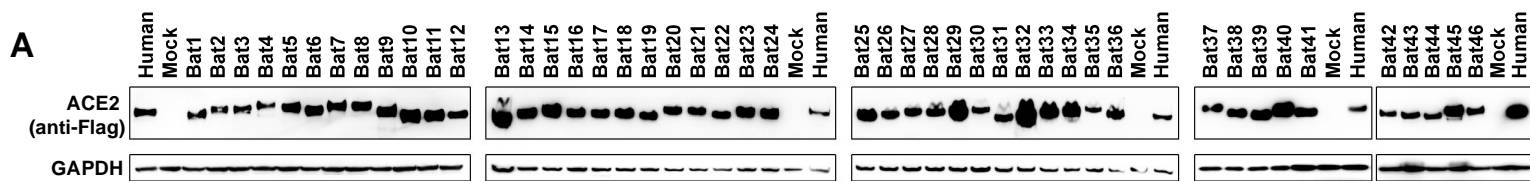
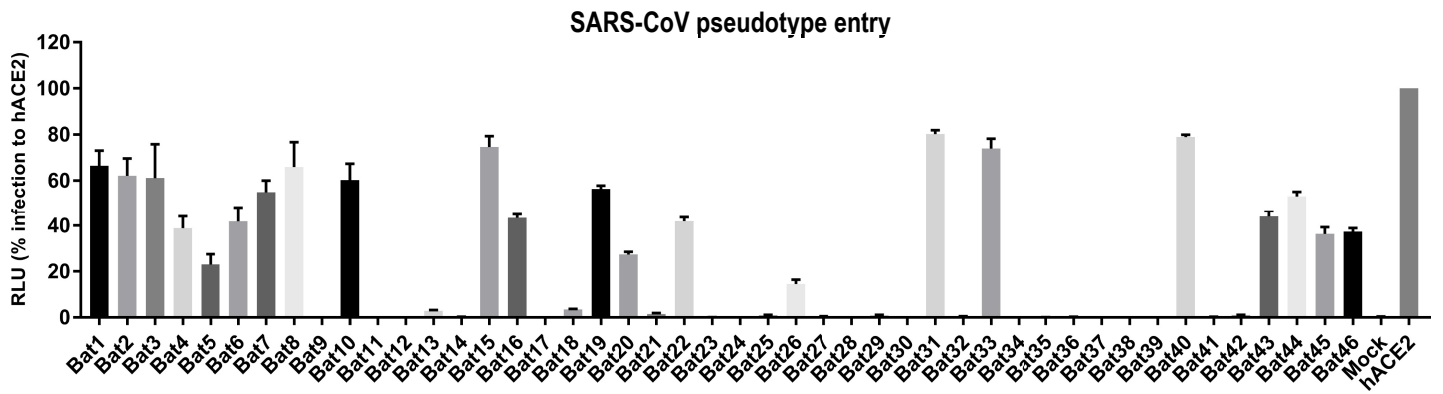


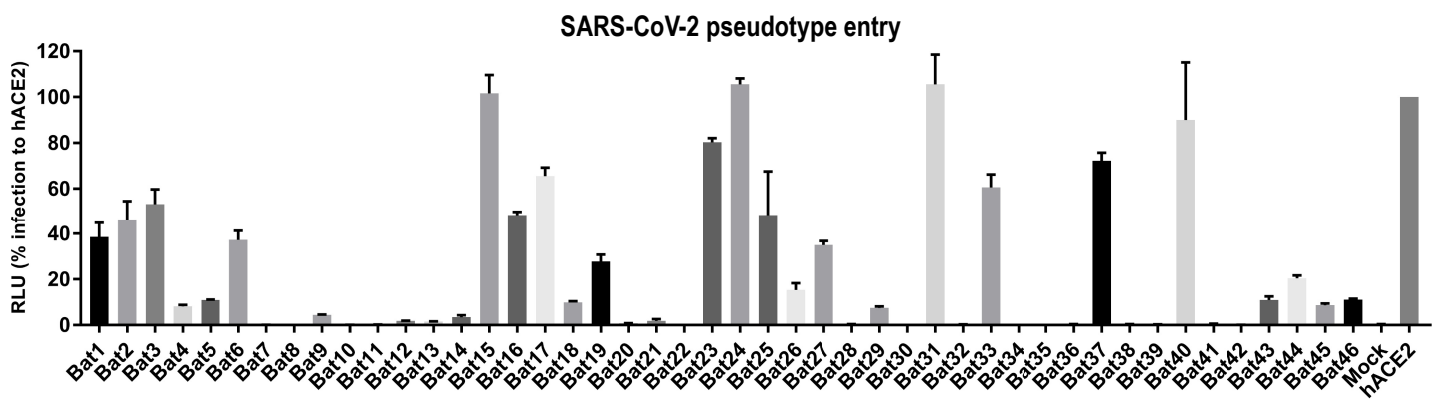
Figure 3

bioRxiv preprint doi: <https://doi.org/10.1101/2020.09.08.284737>; this version posted September 10, 2020. The copyright holder for this preprint (which was not certified by peer review) is the author/funder, who has granted bioRxiv a license to display the preprint in perpetuity. It is made available under a [CC-BY-NC-ND 4.0 International license](https://creativecommons.org/licenses/by-nc-nd/4.0/).

A



B



C

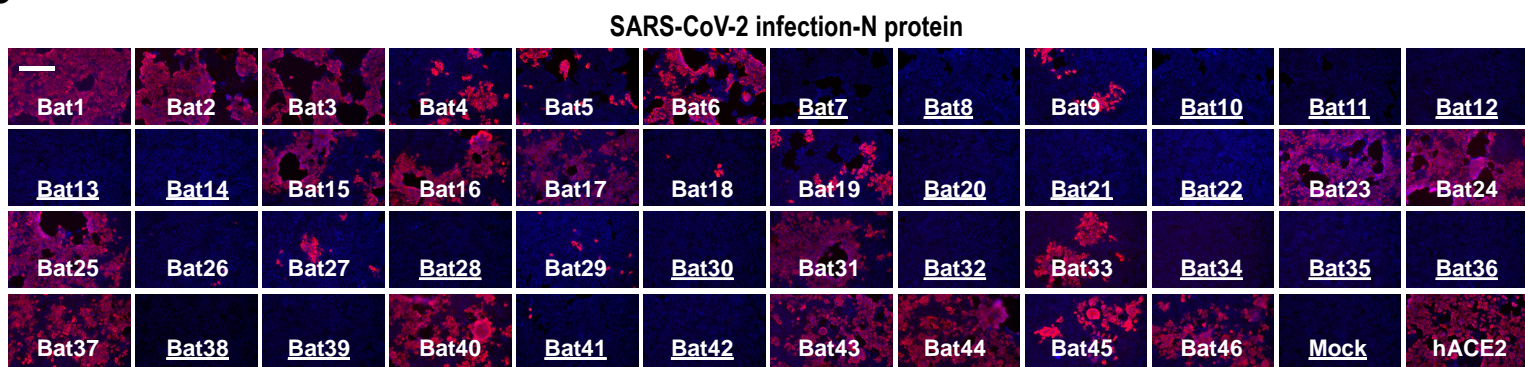


Figure 4

bioRxiv preprint doi: <https://doi.org/10.1101/2020.09.08.284737>; this version posted September 10, 2020. The copyright holder for this preprint (which was not certified by peer review) is the author/funder, who has granted bioRxiv a license to display the preprint in perpetuity. It is made available under aCC-BY-NC-ND 4.0 International license.

